

DUST SPUTTERING BY REVERSE SHOCKS IN SUPERNOVA REMNANTS

BIMAN B. NATH¹, TANMOY LASKAR^{1,2} AND J. MICHAEL SHULL³¹Raman Research Institute, Sadashivanagar, Bangalore 560080, India²St. Stephen's College, Delhi 110007, India³CASA, Department of Astrophysical and Planetary Sciences, University of Colorado, Boulder, CO 80309-0389, USA

biman@rri.res.in, mshull@casa.colorado.edu

Submitted to ApJ ?

ABSTRACT

We consider sputtering of dust grains, believed to be formed in cooling supernovae ejecta, under the influence of reverse shocks. In the regime of self-similar evolution of reverse shocks, we can follow the evolution of ejecta density and temperature analytically as a function of time in different parts of the ejecta, and calculate the sputtering rate of graphite and silicate grains embedded in the ejecta as they encounter the reverse shock. Through analytic (1D) calculations, we find that a fraction of dust mass (1–20% for silicates and graphites) can be sputtered by reverse shocks, the fraction varying with the grain size distribution and the steepness of the density profile of the ejecta mass. It is expected that many more grains will get sputtered in the region between the forward and reverse shocks, so that our analytical results provide a lower limit to the destroyed fraction of dust mass.

Subject headings: ISM : Supernova Remnants, ISM : Dust, Extinction, Galaxies : High-Redshift

1. INTRODUCTION

Understanding the chemical history of heavy elements (“metals”) in the interstellar medium (ISM) of galaxies is an important, but difficult undertaking. Because refractory elements are found to be depleted from the gas phase (locked into grains), they provide a substantial reservoir of coolants in the solid-state phase. Interstellar grain surfaces are believed to furnish formation sites for molecular hydrogen (H₂), which is both a coolant and the starting point for a rich cloud chemistry. Grains also provide a critical transfer mechanism for reprocessing UV/O starlight into far-infrared and sub-mm emission from interstellar molecular clouds and high-redshift galaxies. In the high-redshift universe, the first dust grains may influence the thermodynamics of the primordial gas and thereby control rates of star formation.

Recent observations of dust grains at high redshift have been puzzling in the context of their formation. Several observations of damped Ly α systems (Pettini et al. 1994; Ledoux, Bergeron & Petitjean 2002) have shown evidence of dust grains in them. Also, thermal emission (at 1.2 mm) from dust in high redshift ($z > 6$) QSOs in the Sloan Digital Sky Survey (SDSS) have been reported (Bertoldi et al. 2003). The implied dust mass of $\sim 10^8 M_{\odot}$ within a Gyr after the Big Bang appears difficult to explain with traditional models of grain formation in evolved low mass stars (Dunne et al. 2003), from which grains are thought to be transported to the interstellar medium (ISM) through stellar winds (Whittet 1992).

Recent models have, therefore, focused on other sites of dust grain formation, such as ejecta of core-collapse supernova explosions that can occur on shorter time scales than that of the evolution of low mass stars (Dwek & Scalzo 1980). Core-collapse supernovae are thought to be capable of synthesizing a significant amount of dust in the SN ejecta. Applying a theory of nucleation and grain growth developed by Kozasa & Hasegawa (1987), Kozasa et al.

(1989; 1991) and Todini & Ferrara (2001) have studied grain formation in expanding SN ejecta, the latter estimating the dust mass formed ~ 0.1 – $0.3 M_{\odot}$. Nozawa et al. (2003) have extended it to the case of zero-metallicity SNe for population III stars (see also Schneider, Ferrara & Salvaterra 2004).

Although the SN “dust factory model” would explain the large observed dust masses in high-redshift galaxies, observations of dust in nearby SNe appear inconsistent with this model, falling factors of 10–100 short of the required amounts ($\sim 0.2 M_{\odot}$; see above). As an example, in a review of Type II SN 2003gd (NGC 628), Sugerman et al. (2006) state that “radiative transfer models show that up to 0.02 solar masses of dust has formed within the ejecta”. However, a recent study (Meikle et al. 2007) of the same remnant concludes that the mid-IR flux “is consistent with emission from $4 \times 10^{-5} M_{\odot}$ of newly condensed dust in the ejecta”. In a young, oxygen-rich SNR in the SMC, Stanimirovic et al. (2005) found only $10^{-3} M_{\odot}$ of hot dust ($T_d \approx 120$ K). The claimed sub-mm detection (Dunne et al. 2003) of $\sim 3 M_{\odot}$ of cold dust toward the Cas A remnant was later shown to arise from interstellar dust in an adjacent molecular cloud (Krause et al. 2004).

Observational tests of predictions made by models of SNe are difficult, involving far-IR and sub-mm observations of young SNRs. One must disentangle far-IR backgrounds, separate newly synthesized dust from circumstellar and interstellar dust, and understand the role of SNR reverse shocks, which can destroy newly synthesized dust in high-speed ejecta. A case in point is SN 1987A. Dust formation was inferred in ejecta of SN 1987A, but only $10^{-3} M_{\odot}$ was detected (Dwek 2006; Dwek & Arendt 2007). Additional dust is almost certainly present, because of observed changes in the optical and bolometric fluxes and emission-line asymmetries in the red and blue wings (McCray 1993, 2007). Moreover, the reverse shock has not yet reached the interior of the supernova debris in SN 1987A. These inner ejecta are most prone to dust formation, since

they are cold, dense, and metal-enriched.

A challenging theoretical issue is whether high-velocity dust ($V_{ej} \geq 1000 \text{ km s}^{-1}$) can survive the shocks, thermal sputtering, and grain-grain collisions, as the ejecta are slowed down by the surrounding ISM. A goal of this paper is to determine how much dust survives the SN event and is incorporated into the surrounding ISM. The relative speed of reverse shocks with respect to the expanding ejecta can be very large, and can raise the temperature of the ejecta to the extent of destroying the nascent dust grains in it. It is therefore important to study the effect of reverse shocks in detail.

Recently, Nozawa et al. (2007) have considered this problem and came to the conclusion, with the help of hydrodynamical simulation, that reverse shocks can destroy a fraction of dust mass of order 20–100% depending on the ambient gas density and explosion energy. Bianchi & Schneider (2007) also used numerical simulations and semi-analytical methods to conclude that only a small amount of dust mass survives; e.g., $\sim 7\%$ dust mass survives in the case of a SN with a progenitor of mass $20 M_{\odot}$ and ambient particle density of $\sim 1 \text{ cm}^{-3}$. Nozawa et al. (2007) have included the motion of dust relative to gas within the SN remnant and calculated the evolution of dust grains over a period spanning the radiative phase ($\sim 10^5$ – 10^6 yr), whereas Bianchi & Schneider (2007) neglected the effect of motion of grains on dust destruction and calculated dust evolution up to the non-radiative phase ($\leq 10^5$ yr).

We study in this paper a simple and analytically tractable problem, namely the effect of reverse shocks for a power-law mass distribution of the ejecta, in the regime of self-similar evolution of both forward and reverse shocks. Although the simple formalism does not allow us to study several important processes— including motion of dust grains and its effect on evolution of dust grains— our approach allows one to segregate the processes of destruction within the reverse shock itself from those occurring between forward and reverse shocks (which can be dealt with in numerical simulations involving grain motion).

2. DUST IN SUPERNOVA REMNANTS

We first summarize the results of the theoretical predictions of dust grain formation in SNRs. Todini & Ferrara (2001) calculated the formation of different types of dust grains— amorphous carbon (AC), silicates (enstatites: $MgSiO_3$, forsterites: Mg_2SiO_4) and iron-bearing magnetites (Fe_3O_4) and others, in ejecta with different metallicities. They found that AC grains are generally of larger size, in the range of ~ 0.01 – $0.1 \mu\text{m}$, whereas silicates are produced with sizes $\sim 10^{-3} \mu\text{m}$. Nozawa et al. (2003) reached similar conclusions for Pop III SN events, with sizes of newly synthesized grains spanning a range of three orders of magnitude, with maximum grain size being less than $\sim 1 \mu\text{m}$.

The dust grain parameters in the ISM are inferred to be somewhat different from these estimates. The extinction observations are satisfactorily reproduced by assuming mostly of two components— graphite and silicate— with a common power-law size distribution, $dn/da \propto a^{-3.5}$, truncated at a minimum size $a_l \sim 5 \times 10^{-3} \mu\text{m}$ and a maximum size $a_m \sim 0.25 \mu\text{m}$ (Draine 2003, and references therein).

There also appears to be a population of very small grains with PAH composition. Nozawa et al. (2003) found for grains synthesized in Pop III SN ejecta a size distribution with index -2.5 for smaller grains and with -3.5 for larger grains (with the grain size at crossover point depending on supernovae models). We use these two power laws to bracket the possible size distributions of grains synthesized in SN ejecta, and assume that grains are formed in the range 10^{-7} – $3 \times 10^{-5} \text{ cm}$ (see Figure 11 of Nozawa et al. (2003)). We also consider the case of an upper limit of 10^{-6} cm and compare our results for both upper limits.

It is instructive to estimate the destruction time scales before we calculate the effect of reverse shock in detail. The sputtering time scale for dust (graphite, silicate and iron) grains of size a is approximately $\sim 10^6 \left(\frac{a}{1 \mu\text{m}}\right) \left(\frac{n_e}{1 \text{ cm}^{-3}}\right)^{-1} \text{ yr}$, for ambient temperatures larger than 10^6 K (Draine & Salpeter 1979), where n_e is electron density. For grains with size ~ 0.1 – $0.3 \mu\text{m}$ (which incidentally contain most of the dust mass for a $a^{-3.5}$ distribution), and for $n_e \sim 1$ – 10 cm^{-3} , the sputtering time scale is $\sim 2 \times 10^{4-5} \text{ yr}$.

3. REVERSE SHOCKS

We now briefly discuss the self-similar evolution of forward and reverse shocks in SN (see Truelove & McKee 1999, hereafter referred to as TM99, for further details).

3.1. The ejecta

The parameters used to describe a supernova remnant which affect its evolution are the energy of the explosion (E_{ej}), the mass contained in the expanding ejecta (M_{ej}), the maximum velocity of the material within the ejecta (v_{ej}), and the density of the ISM (ρ_0). Denoting the time of the explosion as $t = 0$, we construct our initial conditions at a later time, still early in the history of the remnant, assuming the ejecta to have already expanded to a radius R_{ej} without any deceleration due to the ambient medium. If we consider SN to be a point explosion, then the radial velocity profile will be linear as ejecta with velocity v will travel out to a distance vt :

$$v(r) = \begin{cases} \frac{r}{t}, & r < R_{ej} \\ 0, & r > R_{ej} \end{cases} \quad (1)$$

This profile becomes flatter as time progresses and the faster-moving ejecta are flung out to greater distances. The corresponding radial density distribution of the ejecta matter is given by:

$$\rho(r) = \begin{cases} \rho_{ej}(v, t) \equiv \frac{M_{ej}}{v_{ej}^3} f\left(\frac{v}{v_{ej}}\right) t^{-3}, & r < R_{ej} \\ \rho_0, & r > R_{ej} \end{cases} \quad (2)$$

where $f(v/v_{ej})$ is the time-independent structure function of the density profile and the t^{-3} term arises from the free expansion of the ejecta. We define a dimensionless parameter to label shells of the ejecta starting from the centre outwards as

$$w = \frac{v}{v_{ej}}, 0 \leq w \leq 1 \quad (3)$$

Following TM99 we consider the situation when f is given by a power law in w :

$$f(w) = \begin{cases} f_0, & 0 \leq w \leq w_c \\ f_n w^{-n}, & w_c \leq w \leq 1 \end{cases} \quad (4)$$

where we have separated the ejecta into a uniform density core region and a power-law envelope region. The continuity of f at w_c and the normalization of ρ translate to expressions for parameters f_0 and f_n in terms of the free parameters w_c and n :

$$\begin{aligned} f_0 &= f_n w_c^{-n} \\ f_n &= \frac{3}{4\pi} \left[\frac{1 - n/3}{1 - (n/3)w_c^{3-n}} \right]. \end{aligned} \quad (5)$$

3.2. Forward and reverse shocks

As the freely expanding ejecta come into contact with the ambient medium, with the contact discontinuity moving at v_{ej} , a speed much larger than the sound speed in the ambient medium, a forward shock is set up in the surrounding gas which propagates into the medium. The ejecta at the contact surface decelerates suddenly as it hits the ambient gas, and consequently, a reverse shock is set up that propagates inwards through the ejecta. While the mass of this matter swept by the forward shock is less than the total mass of the ejecta driving the shock, the remnant is said to be in the *Ejecta Dominated* or ED stage. It is in this stage, before the reverse shock has attained a significant velocity, that the ejecta can be approximated as a spherical piston freely expanding into the ambient gas. When the mass swept by the forward shock becomes approximately equal to the ejecta mass, the corresponding late-time limit is known as the *Sedov-Taylor* or ST stage of the evolution of the remnant.

We follow TM99 to follow the evolution of the reverse shock analytically. Let R_f and R_r denote the radii of the forward and reverse shocks, and $v_f \equiv dR_f/dt$ and $v_r \equiv dR_r/dt$ be the velocities of the forward and reverse shock waves respectively, all in the rest frame of the unshocked ambient medium. We have the velocity of the unshocked ejecta as seen by the reverse shock as it propagates into the ejecta:

$$\tilde{v}_r \equiv v(R_r, t) - v_r(t) = \frac{R_r(t)}{t} - v_r(t). \quad (6)$$

Let ϕ be the ratio of the pressures behind the reverse and forward shock waves and l be the ratio of the radii of the two shocks at a given time:

$$\phi(t) \equiv \frac{\rho_{ej}(v_r, t) \tilde{v}_r^2(t)}{\rho_0 v_f^2(t)}, \quad l(t) \equiv \frac{R_f(t)}{R_r(t)}, \quad w_f(t) \equiv \frac{R_f(t)/t}{v_{ej}}. \quad (7)$$

It is useful to express various parameters in dimensionless forms in the units of characteristic values of these variables. so that, $R_* = R/R_{ch}$, $t_* = t/t_{ch}$, and $v_* = v/v_{ch}$. For example, the characteristic scales of length, time and velocity are given by,

$$\begin{aligned} R_{ch} &= M_{ej}^{1/3} \rho_0^{-1/3} \approx 5.25 n_0^{-1/3} \text{ pc}, \\ t_{ch} &= E^{-1/2} M_{ej}^{5/6} \rho_0^{-1/3} \approx 1.66 \times 10^3 n_0^{-1/3} \text{ yr}, \\ v_{ch} &= R_{ch}/t_{ch} \approx 3.16 \times 10^3 \text{ km s}^{-1}. \end{aligned} \quad (8)$$

(We have assumed $\rho_0 = 1.4n_0m_p$ for He/H=0.1 by number.) We have estimated the numerical values for the case $E = 10^{51}$ erg, $M_{ej} = 10^{34}$ g and $n_0 = 1 \text{ cm}^{-3}$. We will therefore write $R^* = R/R_{ch}$, $t^* = t/t_{ch}$, and $v^* = v/v_{ch}$, and the radius of the reverse shock, in particular, as $R_r^* \equiv R_r/R_{ch}$.

3.2.1. ED (Expansion dominated) stage

The values of ϕ and l approach constant values as $t \rightarrow 0$ if the solutions remain self-similar in the same limit. We write $\phi(t) \simeq \phi(0) \equiv \phi$ and $l(t) \simeq l(0) \equiv l$, and also $w_f(0) = l$. The solution to reverse shock evolution exists in the form of two branches, which we label the *envelope* ($w_c \leq w_f/l_{ED} \leq 1$) and *core* ($0 \leq w_f/l_{ED} \leq w_c$) branches. Denoting $\alpha \equiv \frac{E}{(1/2)M_{ej}v_{ej}^2}$, the evolution of the reverse shock is given by,

$$t^*(R_r^*) = \left(\frac{\alpha}{2}\right)^{1/2} R_r^* \times \begin{cases} \left[1 + \left(\frac{n-3}{3}\right) \left(\frac{\phi}{f_n}\right)^{1/2} l R_r^{*3/2} \right]^{-2/(3-n)}, \\ \left[w_c - \left(\frac{\phi}{l f_0}\right)^{1/2} \left\{ l^{3/2} R_r^{*3/2} - \frac{f_n^{1/2}}{3-n} \left(1 - w_c^{(3-n)/2}\right) \right\} \right]^{-2/3}, \end{cases} \quad (9)$$

where the first part corresponds to the case $w_c \leq w_f/l \leq 1$ and the second part, to $0 \leq w_f/l \leq w_c$. The corresponding velocity of reverse shock in these two cases are,

$$v^*(R_r^*) = \left(\frac{2}{\alpha}\right)^{1/2} \times \begin{cases} \frac{\left[1 - \left(\frac{3-n}{3}\right) \left(\frac{\phi}{f_n}\right)^{1/2} l R_r^{*3/2} \right]^{(5-n)/(3-n)}}{\left[1 + \frac{n}{3} \left(\frac{\phi}{f_n}\right)^{1/2} l R_r^{*3/2} \right]}, \\ \frac{\left[w_c - \left(\frac{\phi}{l f_0}\right)^{1/2} \left\{ l^{3/2} R_r^{*3/2} - \frac{f_n^{1/2}}{3-n} \left(1 - w_c^{(3-n)/2}\right) \right\} \right]^{5/3}}{\left[w_c + \frac{1}{3-n} \left(1 - w_c^{(3-n)/2}\right) \right]}, \end{cases} \quad (10)$$

The relative velocity of the reverse shock in the frame of reference of the expanding ejecta, for the case when the reverse shock is in the envelope region, is given by,

$$\tilde{v}_r^*(R_r^*) = \sqrt{\frac{2\phi}{\alpha f_n}} l R_r^{*3/2} \left(\frac{\left[1 - \left(\frac{3-n}{3}\right) \left(\frac{\phi}{f_n}\right)^{1/2} l R_r^{*3/2} \right]^{2/(3-n)}}{\left[1 + \frac{n}{3} \left(\frac{\phi}{f_n}\right)^{1/2} l R_r^{*3/2} \right]} \right). \quad (11)$$

Note that, since $w_f/l = \frac{R_r(t)/t}{v_{ej}}$ describes the reverse shock, we will define it as ‘ w ’ and use it to label shells in the ejecta.

This solution is valid (in the ED stage) only as long as the reverse shock remains in the envelope $w_{core} \leq w \leq 1$. In the case of $n < 3$ ejecta, there is no need for a core and we can take the limit $w_{core} \rightarrow 0$. For $n > 3$ however, we must have a ‘‘flat profile’’ core to keep the integrated mass finite. For the steep index scenario, therefore, the functional form of the solution will change when the reverse shock reaches the core and we will return to this point later.

3.2.2. ST (Sedov-Taylor) stage

We now describe the Sedov-Taylor stage, which is the late-time evolution limit of the non-radiative phase of a supernova remnant. Following TM99, we assume that the shocks trace a constant acceleration path after transition to the ST stage at t_{ST} , which (approximately) begins when the mass of the ambient medium shocked by the forward shock equals the mass ejected by the supernova. Thus the velocity of the oncoming ejecta in the frame of the reverse shock is

$$\tilde{v}_r^*(t^*) = \tilde{v}_{r,ST}^* + \tilde{a}_{r,ST}^*(t^* - t_{ST}^*), \quad (12)$$

where $\tilde{a}_{r,ST}$ is the constant acceleration and $\tilde{v}_{r,ST}$ is the velocity of the ejecta w.r.t the reverse shock at t_{ST} . Note that $\tilde{v}_r = -td(R_r/t)/dt$. Using this and integrating the resulting expression from t_{ST} to t gives

$$R_r^*(t^*) = t^* \left[\frac{R_{r,ST}^*}{t_{ST}^*} - \tilde{a}_{r,ST}^*(t^* - t_{ST}^*) - (\tilde{v}_{r,ST}^* - \tilde{a}_{r,ST}^* t_{ST}^*) \ln \left(\frac{t^*}{t_{ST}^*} \right) \right] \quad (13)$$

For the $n < 3$ case, we therefore have an implicit solution for the reverse shock position in the ED stage $t < t_{ST}$ and an explicit solution in the form of a uniform acceleration description in the ST stage. For the $n > 5$ case, we again have an implicit solution in the ED stage at least while $t < t_{core}$. In fact, an explicit solution for $R_r^*(t^*)$ can be determined from the implicit solution in the ED stage for $n > 5$ remnants. We have (see equation (74) of TM99),

$$t^*(R_r^*) = \left(\frac{\alpha}{2} \right)^{1/2} R_r^* \left[1 + \left(\frac{n-3}{3} \right) \left(\frac{\phi}{f_n} \right)^{1/2} l R_r^{*3/2} \right]^{-2/(3-n)} \quad (14)$$

In this expression, we can take the limit $w_{core} \rightarrow 0$ by allowing $v_{ej} \rightarrow \infty$, the ejecta energy E remaining finite. In this limit $f_n \rightarrow 0$ and when the second term in the brackets becomes much larger than unity, we have

$$R_r^*(t^*) = \left[\frac{27}{4\pi n(n-3)l^2\phi} \left\{ \frac{10}{3} \left(\frac{n-5}{n-3} \right) \right\}^{\frac{n-3}{2}} \right]^{1/n} (t^*)^{\frac{n-3}{n}}. \quad (15)$$

This gives us the velocity of the reverse shock as,

$$v_r^*(t^*) = \frac{n-3}{n} \left[\frac{27}{4\pi n(n-3)l^2\phi} \left\{ \frac{10}{3} \left(\frac{n-5}{n-3} \right) \right\}^{\frac{n-3}{2}} \right]^{1/n} (t^*)^{-1/n} \quad (16)$$

and correspondingly,

$$\begin{aligned} \tilde{v}_r^*(t^*) &= \frac{R_r}{t} - v_r^* \\ &= \frac{3}{n} \left[\frac{27}{4\pi n(n-3)l^2\phi} \left\{ \frac{10}{3} \left(\frac{n-5}{n-3} \right) \right\}^{\frac{n-3}{2}} \right]^{1/n} t^{*-1/n} \end{aligned} \quad (17)$$

This is the result arrived at by Chevalier (1982) and Nadyozhin (1985) - henceforth referred to as 'the CN solution'. The transition of a supernova remnant with $n > 5$ to this stage has been shown to occur extremely fast (TM99). Thus for all practical purposes, we may assume that the remnant begins with the CN stage.

The reverse shock then moves into the core at $t = t_{core}$. TM99 assumed that the reverse shock motion after this time is also described by a Sedov-Taylor trajectory - which leads to better match between the two regimes in terms of continuity of the shock radius and velocity. In the case of $n > 5$, therefore, if we replace t_{ST} by t_{core} in the ST stage equations above, the same analysis follows through. The numerical values of the parameters t_{core} , $\tilde{a}_{r,core}$ and $\tilde{v}_{r,core}$ are, of course, different from the parameters for the $n < 3$ case: viz t_{ST} and $\tilde{a}_{r,ST}$. We have,

$$\begin{aligned} R_r^*(t^*) &= t^* \left[\frac{R_{r,core}^*}{t_{core}^*} - \tilde{a}_{r,core}^*(t^* - t_{core}^*) \right. \\ &\quad \left. - (\tilde{v}_{r,core}^* - \tilde{a}_{r,core}^* t_{core}^*) \ln \left(\frac{t^*}{t_{core}^*} \right) \right] \\ \tilde{v}_r^*(t^*) &= \tilde{v}_{r,core}^* + \tilde{a}_{r,core}^*(t^* - t_{core}^*). \end{aligned} \quad (18)$$

The values of the parameters used in our calculations have been taken from TM99, which have been checked with results from simulations.

3.2.3. Summary of ED and ST solutions

We thus have the final solutions for the reverse shock as follows. In the case of $n < 3$, equations (9; first part) and (11) describe the solutions in the ED stage, and, thereafter, equations (13) and (12) are appropriate for solutions in the ST stage. For the case of $n > 5$, solutions are given by equations (15) and (17) in the $t < t_{core}$ stage. Afterwards, in the $t > t_{core}$ stage, equations (18) describe the solutions. The analytical solutions remain valid until $t_* \sim 2.2$ (TM99), and we calculate the evolution of shocks until this point (except for $n = 4$; see below).

For a given set of values of E and M_{ej} , we can therefore solve for reverse shock position and relative velocity, assuming a density distribution described by index n . The parameter α in different cases of n , is given by,

$$\alpha \equiv \frac{E}{(1/2)M_{ej}v_{ej}^2} = \left(\frac{3-n}{5-n} \right) \left(\frac{w_{core}^{-(5-n)} - n/5}{w_{core}^{-(3-n)} - n/3} \right) w_{core}^2, \quad (19)$$

For $n < 3$, we calculate this in the limit of $w_{core} = 0$, and for $n > 5$ (including the case of $n = 4$) we assume (following TM99) a value of $w_{core} = 0.1$. Values of other parameters (such as l, ϕ) are taken from appropriate tables of TM99 for the relevant values of n .

We also consider the special case of $n = 4$, for which the mass integral diverges without a core. We follow the prescriptions of TM99 (their section 8) for this case (and, again, assume $w_{core} = 0.1$), and track the reverse shock with only ED solution without any transition to the ST case. According to TM99, based on their comparison of analytical and numerical results, this prescription gives tolerably good results (accurate to within 24%) until $t^* = 1.2$.

3.3. Arrival time of reverse shock

We have introduced a label to a given shell in the supernova ejecta by $w \equiv w_f/l = \frac{R_r(t)/t}{v_{ej}}$, the ratio of the velocity of the ejecta in the shell to the maximum ejecta velocity. The ejecta in a shell specified by a given w first undergoes free expansion (in the ED stage) and self-similar expansion (in the ST stage) until hit by the incoming reverse shock wave. This occurs at a time, which we call t_{hit} , which is a function of w and which is found by equating w to the v_r/v_{ej} found from the position of the reverse shock. That is,

$$w = \frac{v_r}{v_{ej}} = \frac{R_r}{R_{ej}} \Rightarrow R_r = w R_{ej} = w v_{ej} t_{hit}. \quad (20)$$

Or, in terms of dimensionless variables,

$$R_r^* = w \cdot \frac{v_{ej} t_{hit}}{R_{ch}} = \left(w \cdot \frac{v_{ej} t_{ch}}{R_{ch}} \right) t_{hit}^*. \quad (21)$$

This expression for R_r^* in terms of t^* is equated to the explicit solution for the reverse shock, when available, as a function of time, and the resultant linear equation in t_{hit}^* and w is solved using the bisection method for each given w . This is applicable to the steep ($n > 5$) ejecta case (both the CN and ST stage) as well as to the ST stage for

shallow ($n < 3$) ejecta. For the ED stage of shallow ejecta, we use t_{hit}^* as a function of R_r^* in equation (9) and then employ the bisection method exactly as before to solve for t_{hit}^* . Either way, we can determine t_{hit}^* given any shell labeled by a w in the SN ejecta.

3.4. Density and temperature evolution in ejecta shells

We assume that gas in a given shell of the ejecta evolves adiabatically before t_{hit} . The temperature is then raised to the postshock temperature and the density acquires a jump, corresponding to the value of relative shock velocity \tilde{v}_r . After t_{hit} , the gas again evolves adiabatically, that is, its density decreases as t^{-3} (equation 2). Its temperature decreases as $T \propto \rho^{\gamma-1} \propto t^{-2}$, for $\gamma = 5/3$ appropriate for monoatomic gas. For a shell with a certain value of w , therefore, we have the following evolution of density,

$$\rho(t, w) = \begin{cases} \frac{M_{ej}}{v_{ej}^3} f(w) t^{-3}, & t < t_{hit} \\ 4 \frac{M_{ej}}{v_{ej}^3} f(w) t^{-3}, & t_{hit} \leq t < 2.2t_{ch} \end{cases} \quad (22)$$

and temperature,

$$T(t, w) = \begin{cases} T_i (\frac{t}{t_i})^{-2}, & t < t_{hit} \\ T_{rshock} (\frac{t}{t_{hit}})^{-2}, & t_{hit} \leq t < 2.2t_{ch} \end{cases} \quad (23)$$

where $T_{rshock} = \frac{3}{16} \mu m_p \tilde{v}_r^2 / k_B$, the post-shock temperature due to the reverse shock with relative velocity \tilde{v}_r . For a completely ionized gas the mean molecular weight $\mu = 0.6$. We assume a value of $T_i = 5400$ K at $t_i = 70$ days, motivated by photometric observations of SN1987A (Catchpole et al. 1987) where it was estimated that the photospheric temperature at ~ 70 d after the explosion was ~ 5400 K. We have also checked that our results do not depend strongly on these assumptions.

3.5. Sputtering of dust

Given the above mentioned evolution of density and temperature in shells of ejecta labeled by different values of w , we can compute the steady decrease in grain radius, for different types of dust grains. We use the polynomial fit given by Tielens et al (1994) for graphites and silicates as a function of gas temperature. They expressed the rate, $(1/n_H) \frac{da}{dt}$ in powers of $\log_{10} T$, with coefficients for different grain composition tabulated in their Table 4 (see their equation 4.21). These rates are consistent with recent results of Nozawa et al. (2006).

We follow a shell of ejecta material labeled by a value $0 < w < 1$ from ~ 10 years after the explosion (by which time dust grains are believed to have formed in the cooling ejecta, since the formation time scale is of order a few years (see, e.g., Todini & Ferrara 2001)), to when the reverse shock hits the shell at t_{hit} and beyond, until a time $t^* \sim 2.2$, which is the limit of the validity of the analytical solutions.

4. RESULTS

We have calculated the effect of reverse shocks on sputtering of graphite and silicate grains for typical value of explosion energy, stellar ejecta mass and ambient density. Below we show the results for $E = 10^{51}$ erg, $M_{ej} = 10^{34}$ g, $\rho_0 = 10^{-24}$ g cm $^{-3}$.

First, we show the evolution of grain radius (for graphites and silicates) for two dust grains embedded in

two particular shells, for example, in ejecta characterized by $n = 0$ and $E = 10^{51}$ erg. We show in Figure 1 the cases for the shells marked $w = 0.3$, and 0.6 . The reverse shock passes through these two shells, first hitting the $w = 0.6$ shell at $\sim 0.5t_{ch} \sim 0.8 \times 10^3 n_0^{-1/3}$ yr, and then the $w = 0.3$ shell at $\sim 1.2t_{ch} \sim 2 \times 10^3 n_0^{-1/3}$ yr. The bottom panel of Figure 1 shows the rise in temperature for these two shells followed by adiabatic cooling. Initially the temperature drops to very low temperatures due to strong adiabatic cooling, although, in reality, gas cannot be cooled below the temperature of the cosmic microwave background, but we have not used such a lower bound in our calculations. At any rate, the post-shock temperature does not depend on the low temperature of the gas upstream, being determined only by the strength of the reverse shock, and so the results of our calculation remains realistic in spite of the strong cooling before the reverse shock hits the gas in a given shell.

Figure 2 plots the ratio of final to initial grain sizes as a function of the initial grain sizes for silicates and graphites forming (and being sputtered) in shells $w = 0.2, 0.4, 0.6$ for the particular case of $n = 0$. *Since the sputtering yield of silicate grains is larger than that of graphites for a given set of parameters*, silicates are eroded more rapidly than graphite grains for sputtering in a given ejecta shell. Also, the relatively outer shell of $w = 0.6$ experiences less sputtering than the inner shells of $w = 0.2$ and 0.4 . This is expected since the reverse shock (relative) speed picks up as it plows through the ejecta, increasing with decreasing values of w . To illustrate this point, we plot the trend of the relative velocity of the reverse shock as a function of w for the shells hit by the shock in Figure 3, for $n = 0$ (solid), $n = 2$ (dotted), and $n = 6$ (dashed). The relative velocity is a rising function with decreasing w , for $n = 0$ and for $n > 5$, and it is a peaked function for $n = 2$ (and also for $n = 4$, which is not shown here, but as shown by TM99).

However, we notice in Figure 2 that grains (both graphites and silicates) in shell $w = 0.2$ (solid curve) are sputtered to a somewhat lesser extent than grains in the $w = 0.4$ shell, although the relative speed of the reverse shock should be (according to Figure 3, solid curve for $n = 0$) higher when it hits the $w = 0.2$ shell than at the $w = 0.4$ shell. Although the post-shock temperature at $w = 0.2$ is higher than at $w = 0.4$, the shells in the inner region encounter the reverse shock later than shells in the outer region of ejecta, and by the time they encounter it, the density in the inner shells would have decreased rapidly (see equation 22). The rarefaction in the inner shells at the time of encounter with the reverse shocks lessens the effect of dust sputtering in these shells.

We illustrate this point by considering grains which are sputtered below a certain size, say, 10^{-7} cm (10^{-3} μm), as a function of the shell in which they reside (and get sputtered). We determine the maximum size of grains which are sputtered below a size $\sim 10^{-7}$ cm, as a function of w , for different shells, and present the results in Figure 4. Curves for different values of n show the maximum size of grains sputtered below $0.001 \mu\text{m}$ as a function of the parameter w (left panels), as well as against the fraction of ejecta mass that is contained inside of the concerned shell, $M(< w)/M_{ej}$ in the right panels. Results for graphites

and silicate grains are shown in the upper and lower panels respectively.

Figure 4 clearly shows that sputtering becomes intense in intermediate shells, and decreases (as a result of rarefaction) with decreasing value of w for small values of w . The sizes of grains which are sputtered below $10^{-3}\mu\text{m}$ lie in the range of $\leq 10^{-3}\mu\text{m} - 10^{-2.6}\mu\text{m}$, with silicates more strongly sputtered than graphites. In all cases, the curves of the maximum size of sputtered grains increases with decreasing values of w and $M(<w)/M_{ej}$, finally plunging to very low values for $w \ll 1$, indicating negligible effect of the reverse shock deep inside the ejecta. For example, the (dotted) curve for $n = 2$ shows a peak at $w \sim 0.17$ below which the maximum size of sputtered grains decreases.

Also, although it is not explicitly shown in Figure 4, the corresponding results for $n > 5$ show that reverse shocks do not penetrate most of the ejecta mass in the time period of the validity range of analytical solutions $t_* \sim 2.2$. Analytical means allow us to probe deep into the ejecta mass distribution only for $n < 3$, and full hydrodynamical models are needed to address the cases of steeper profiles. For steep density distributions, the limiting time of $t = 2.2t_{ch}$ is reached by the time the reverse shock only skims the surface of the ejecta, as far as mass fraction is concerned. The characteristic time in the case considered here ($E = 10^{51}$ erg, $M_{ej} = 10^{34}$ g, ambient density $\rho_0 = 10^{-24}$ g cm $^{-3}$) is $t_{ch} \sim 1.7 \times 10^3$ yr. Although, by the limiting time of $2.2t_{ch} \sim 3.7 \times 10^3$ yr for the validity of self-similar regime, reverse shocks can hit shells with small w in these steep cases, the mass contained inside of these shells remains very large. In other words, in these cases we cannot probe what happens to most of the ejecta mass, or the dust contained in them with analytical means, within the limits of the self-similar regime of shock evolution.

We also note that a substantial amount of grain sputtering takes place in the hot gas between the forward and reverse shock that analytical methods cannot capture. Detailed hydrodynamical calculations are needed to address these issues, and our result can only provide a lower limit to the total mass fraction of dust that is destroyed.

Finally, we calculate the total dust mass sputtered away as a function of initial grain sizes in the following manner. We first calculate for a given shell w , the final grain size $a_f(a_i, w)$ corresponding to the initial grain size a_i . Then the fraction $1 - (a_f/a_i)^3$ is the total dust mass sputtered for grains formed in this shell. We then calculate the total dust mass sputtered for all shells (for a given initial grain size a_i), weighted by the shell mass in which they are situated, as given by,

$$f_d(a_i) = \int [1 - (a_f/a_i)^3] \frac{dM(<w)}{M_{ej}}, \quad (24)$$

where $M(<w)$ is the ejecta mass contained within the shell w .

We plot these weighted fractions $f_d(a_i)$ for graphite and silicate grains as functions of a_i for $n = 0, 2, 4$ in Figure 5. Thick curves denote the results for silicates and thin ones are for graphite grains. As expected, the sputtered fraction decreases with increasing a_i , and the fraction for silicates is in general larger than that for graphites.

The total dust mass fraction that is destroyed can then be evaluated from these results by convolving $f_d(a_i)$ with an initial grain size distribution. As mentioned earlier,

Nozawa et al. (2003) found that the size distribution of synthesized grains is bounded by two power laws, with indices -3.5 for larger grains and -2.5 for smaller grains. We therefore estimate the total dust mass fraction destroyed, assuming a size distribution $n(a)da \propto a^{-p}da$, with $p = 2.5$ and 3.5 . The destroyed fraction of dust mass is given by,

$$f = \frac{\int n(a)a^3 f_d(a)da}{\int n(a)a^3 da}, \quad (25)$$

where the grain volume scales as a^3 . The results for graphites and silicates are presented in Table 1, for $n = 0, 2, 4$ ($E = 10^{51}$ erg, $M_{ej} = 10^{34}$ g), leaving the cases of $n > 5$ for which the reverse shocks do not reach the interiors of the ejecta within the validity range of self-similar solutions. We assume the lower and upper limit for the integral to be 10^{-7} cm and 3×10^{-5} cm respectively, as explained earlier in §2. We also calculate the destroyed fractions for a truncated grain size distribution, with an upper limit of 10^{-6} cm, and the results are shown inside brackets in Table 1 for comparison.

We have further studied the variation of the destroyed dust mass fraction with explosion energy and ejected mass. Tables 2 and 3 show the fraction of dust mass sputtered for two sets of parameters: Table 2 for $M_{ej} = 10^{34}$ g and $E = 10^{52}$ erg, and Table 3 for $M_{ej} = 2 \times 10^{34}$ g and $E = 10^{51}$ erg. Figure 6 plots the variation of (logarithm) of the destroyed dust mass fraction, f , for silicates, for different values of explosion energy and ejected mass, and for different mass profiles ($n = 0, 2, 4$). In the upper panel, we plot the variation of f with M_{ej} (in logarithm), keeping the explosion energy constant at $E = 10^{51}$ erg, and in the lower panel, we plot (logarithms of) f with explosion energy E , keeping the ejected mass fixed at $M_{ej}10^{34}$ g. The destroyed fraction generally increases with ejected mass, but its variation with explosion energy is not monotonic. The reason is that the process of dust destruction depends mainly on two factors: the speed of the reverse shock (which depends on the characteristic speed v_{ch}) and the characteristic time, t_{ch} . Now, $v_{ch} \propto M_{ej}^{-1/2}E^{1/2}$, whereas $t_{ch} \propto M_{ej}^{5/6}E^{-1/2}$. It would appear that a change in ejected mass manifests itself in increasing t_{ch} , and thereby increasing the destroyed fraction, whereas, a change in E affects t_{ch} and v_{ch} in a complicated manner, which results in the variation shown in the bottom panel of Figure 6.

5. DISCUSSION

We therefore find that a mass fraction $\leq 20\%$ of silicates and graphite grains created in cooling ejecta can be sputtered away by the reverse shock if the density distribution of the ejecta has a shallow profile ($n < 5$). Nozawa et al (2007) recently studied sputtering of dust in reverse shock and found a destroyed dust mass fraction of 0.2–1; their result for an ambient hydrogen number density of 1 cm^{-3} and a progenitor mass of $13 M_\odot$ is ~ 0.7 (their Table 1). In fact, their result for the ‘unmixed grains’ model (which has to do with spatial mixing of the core heavy-element distribution) in which the maximum size is $0.01\mu\text{m}$ is ~ 0.5 . It should be noted, however, that a considerable amount of sputtering in their calculation is caused by the hot plasma between the forward and the reverse shocks (see §3.3 in Nozawa et al (2007)), which we have not considered. In our case, for analytical simplicity, we have assumed the

post-reverse shocked gas to be cooling adiabatically. Our results are, therefore, expected to give lower bounds on the actual dust mass fraction destroyed in SN remnants.

There is another reason why the destroyed fraction of dust mass calculated here is lower than that of Nozawa et al (2007) and Bianchi & Schneider (2007). Strictly speaking, the destruction rate of Tielens et al (1994) used here is valid for a gas with solar abundance. The gas in the dust formation region in the supernova ejecta is expected to be metal rich, and the destruction of dust grains in this gas can be more efficient in this case, since sputtering yields by metal ions are much higher in general than by hydrogen and helium ions.

It should be noted that our results for the destroyed fraction is independent of the ambient density, since the gas density enters into our calculation only to change t_{ch} (notice in equations 8 that v_{ch} is independent of ambient density, and so the relative speed of reverse shock, and in turn the post-shock temperature, are also independent of ambient density). In reality, however, a lot of grain sputtering would take place between the forward and reverse shock, where the gas density will crucially depend on the ambient density. This aspect of grain sputtering is neglected in our analytical calculation, but is captured in the simulation results of Bianchi & Schneider (2007) and Nozawa et al. (2007).

Another difference between our results and those of Bianchi & Schneider (2007) arises from the assumption of initial grain size distribution. Bianchi & Schneider (2007) used grains of small size in their calculation, with silicate grains smaller than $\leq 0.01 \mu\text{m}$ and graphites smaller than $\leq 0.05 \mu\text{m}$. Also, their size distribution is more confined to a narrow range than the power law distribution assumed here. Both these factors would enhance the destroyed fraction of dust mass in reverse shocks. For example, if the sizes of SiO_2 grains have a delta-function distribution around $a_i \sim 25 \text{ \AA}$ (see Figure 1 of Bianchi & Schneider 2007), then the curves in Figure 2 of the present paper (say, for $w = 0.2$) yield a mass destruction fraction of $\sim 22 \%$ (with $a_f/a_i \sim 0.92$). For $M_g SiO_3$ grains of size $\sim 45 \text{ \AA}$, we similarly estimate a destroyed mass fraction of $\sim 14 \%$. From Figure 2, we estimate that one requires $a_f \sim 10 \text{ \AA}$ in order to get $\sim 50\%$ destruction of silicate grains.

A note on the observed density distribution of supernovae ejecta is in order here. Chevalier & Fransson (1994) studied a model of the ejecta from a Type II supernova with a shallow ($n < 3$) core surrounded by a steep ($n > 5$) envelope. In the case of Type Ia supernovae, a steep density distribution in the ejecta mass has also been discussed in the literature (Colgate & McKee (1969); Dwarkadas & Chevalier (1997)). There has been success, however, in modelling data of Type Ia supernova with uniformly distributed ($n \sim 0$) ejecta (Hamilton & Sarazin (1984); Hamilton, Sarazin & Szymkowiak (1986)).

It is worth considering what observations might improve our understanding of the net dust production by SNe. Far-infrared and sub-millimeter observations of reverse-shocked dust in young SNe by *Spitzer*, *Herschel*, and other facilities will help, but our theoretical studies suggest that unshocked (cold) dust may harbor a considerable mass of undetected dust. To constrain this dust and distinguish it

from surrounding interstellar clouds will probably require sub-mm observations with small beam sizes. This brings in complications of the circumstellar environment of young SNe. Furthermore, the long times (thousands of years) required for reverse shocks to reach the core ejecta suggest that late-time observations of supernova remnants would be useful.

6. SUMMARY

We have studied the effect of reverse shocks analytically, in the regime of self-similar evolution, on the sputtering of dust grains that are believed to form in cooling ejecta. For representative cases we found that fractions of dust mass that is destroyed are of order of order 1–20 % of silicates and graphites, for SN of explosion energy $\sim 10^{51}$ erg, ejecta mass $\sim 10^{34}$ g, and an ambient density $\sim 10^{-24}$ g cm^{-3} . Our analytical formalism provides only a lower bound on the dust mass fraction that is destroyed by the reverse shock, since it ignores further sputtering of grains in hot plasma between the forward and reverse shocks. Our results are, therefore, consistent with the recent estimates from numerical simulations which include these additional effects. Furthermore, Our study provides a formalism to generalize these results to cases with different values of SN parameters.

We thank Drs. R. Chevalier, E. Dwek, T. Nozawa, A. Ray and Y. Shchekinov for helpful discussions. This work was supported at the University of Colorado by NASA Theory grant NNX07-AG77G and NSF theory grant AST07-07474.

REFERENCES

- Bertoldi, F., Carilli, C. L., Cox, P., Fan, X., Strauss, M. A., Beelen, A., Omont, A. & Zylka, R. 2003, *A&A*, 406, L55
- Bianchi, S. & Schneider, R. 2007, *MNRAS*, 378, 973
- Catchpole, R. M. et al., *MNRAS*, 229, 15
- Chevalier, R. A. 1982, *ApJ*, 258, 790
- Colgate, S. A. & McKee, C. 1969, 157, 623
- Deneault, E. A., Clayton, D. D. & Heger, A. 2003, *ApJ*, 594, 312
- Dunne, L., Eales, S., Ivison, R., Morgan, H., Edmunds, M. 2003, *Nature*, 424, 285
- Dwek, E. 2006, *Science*, 313, 178
- Dwek, E., & Arendt, R. G. 2007, in *AIP Conf. Proc., Supernova 1987A: 20 Years After*, ed. S. Immler, K. Weiler, R. McCray, Vol. 937, 58
- Dwek, E., & Werner, M. W. 1981, *ApJ*, 248, 138
- Gerardy, C. L., Fessen, R. A., Höfflich, P. & Wheeler, J. C. 2000, *AJ*, 119, 2968
- Gerardy, C. L. et al. 2002, *ApJ*, 575, 1007
- Hamilton, A. J. S. & Sarazin, C. L. 1984, *ApJ*, 281, 682
- Hamilton, A. J. S., Sarazin, C. L. & Szymkowiak, A. E. 1986, *ApJ*, 300, 698
- Kozasa, T., Hasegawa, H. & Nomoto, K. 1989, *ApJ*, 344, 325
- Krause, O., et al. 2004, *Nature*, 432, 596
- Ledoux, C., Bergeron, J., Petitjean, P. 2002, *A&A*, 385, 802
- McCray, R. 1993, *ARA&A*, 31, 175
- McCray, R. 2007, in *AIP Conf. Proc., Supernova 1987A: 20 Years After*, ed. S. Immler, K. Weiler, R. McCray, Vol. 937, 3
- Meikle, W.P.S., Mattila, S., et al. 2007, *ApJ*, 665, 608
- Morgan, H. L. & Edmunds, M. G. 2003, *MNRAS*, 343, 427
- Moseley, S. H., Dwek, E., Giaccum, W., Graham, J. R., Loewenstein, R. F., Silverberg, R. F. 1989, *Nature*, 340, 697
- Nadyozhin, D. K. 1985, *Ap&SS*, 112, 225
- Nozawa, T., Kozasa, T., Umeda, H., Maeda, K. & Nomoto, K. 2003, *ApJ*, 598, 785
- Nozawa, T., Kozasa, T., Habe, A. 2006, *ApJ*, 648, 435
- Nozawa, T. et al. 2007, *astro-ph/0706.0383*
- Pettini, M., Smith, L. J., Hunstead, R. W. & King, D. L. 1994, *ApJ*, 426, 79
- Schneider, R., Ferrara, A. & Salvaterra, R. 2004, *MNRAS*, 351, 1379
- Seab, C. G. & Shull, J. M. 1983, *ApJ*, 275, 652
- Shull, J. M. 1978, *ApJ*, 226, 858
- Stanimirovic, S., et al. 2005, *ApJ*, 632, L103
- Sugerman, B. E. K. et al. 2006, *Science*, 313, 196
- Tielens, A. G. G. M., McKee, C. F., Seab, C. G. & Hollenbach, D. J., 1994, *ApJ*, 431, 321
- Todini, P. & Ferrara, A. 2001, *MNRAS*, 325, 726
- Truelove, J. K. & McKee, C. F. 1999, *ApJ*, 120, 299 (TM99)
- Whittet, D. C. B. 1992, *Dust in the Galactic Environment*, IOP Publishing, Great Britain.

Table 1 : Fraction of dust mass sputtered for sizes ranging from $10^{-4} \mu\text{m}$ to $a_{max} = 0.3 \mu\text{m}$ (or $a_{max} = 0.01 \mu\text{m}$)

grain (dn/da)	$n = 0$	$n = 2$	$n = 4$
Graphite ($\propto a^{-3.5}$)	0.004 (0.02)	0.01 (0.05)	0.007 (0.04)
($\propto a^{-2.5}$)	6×10^{-4} (0.01)	0.001 (0.03)	0.001 (0.03)
Silicate ($\propto a^{-3.5}$)	0.01 (0.07)	0.03 (0.13)	0.02 (0.10)
($\propto a^{-2.5}$)	0.002 (0.05)	0.005 (0.10)	0.004 (0.07)

Table 2 : Fraction of dust mass sputtered for $M_{ej} = 10^{34}$ g, $E_{ej} = 10^{52}$ erg.

grain (dn/da)	$n = 0$	$n = 2$	$n = 4$
Graphite ($\propto a^{-3.5}$)	0.001 (0.008)	0.003 (0.01)	0.005 (0.03)
($\propto a^{-2.5}$)	2×10^{-4} (0.005)	4×10^{-4} (0.01)	7×10^{-4} (0.02)
Silicate ($\propto a^{-3.5}$)	0.006 (0.03)	0.01 (0.06)	0.05 (0.16)
($\propto a^{-2.5}$)	0.001 (0.02)	0.002 (0.04)	0.018 (0.14)

Table 3 : Fraction of dust mass sputtered for $M_{ej} = 2 \times 10^{34}$ g, $E_{ej} = 10^{51}$ erg.

grain (dn/da)	$n = 0$	$n = 2$	$n = 4$
Graphite ($\propto a^{-3.5}$)	0.006 (0.035)	0.015 (0.08)	0.01 (0.06)
($\propto a^{-2.5}$)	10^{-3} (0.02)	0.003 (0.06)	0.002 (0.04)
Silicate ($\propto a^{-3.5}$)	0.02 (0.1)	0.04 (0.18)	0.03 (0.13)
($\propto a^{-2.5}$)	0.003 (0.07)	0.008 (0.14)	0.005 (0.10)

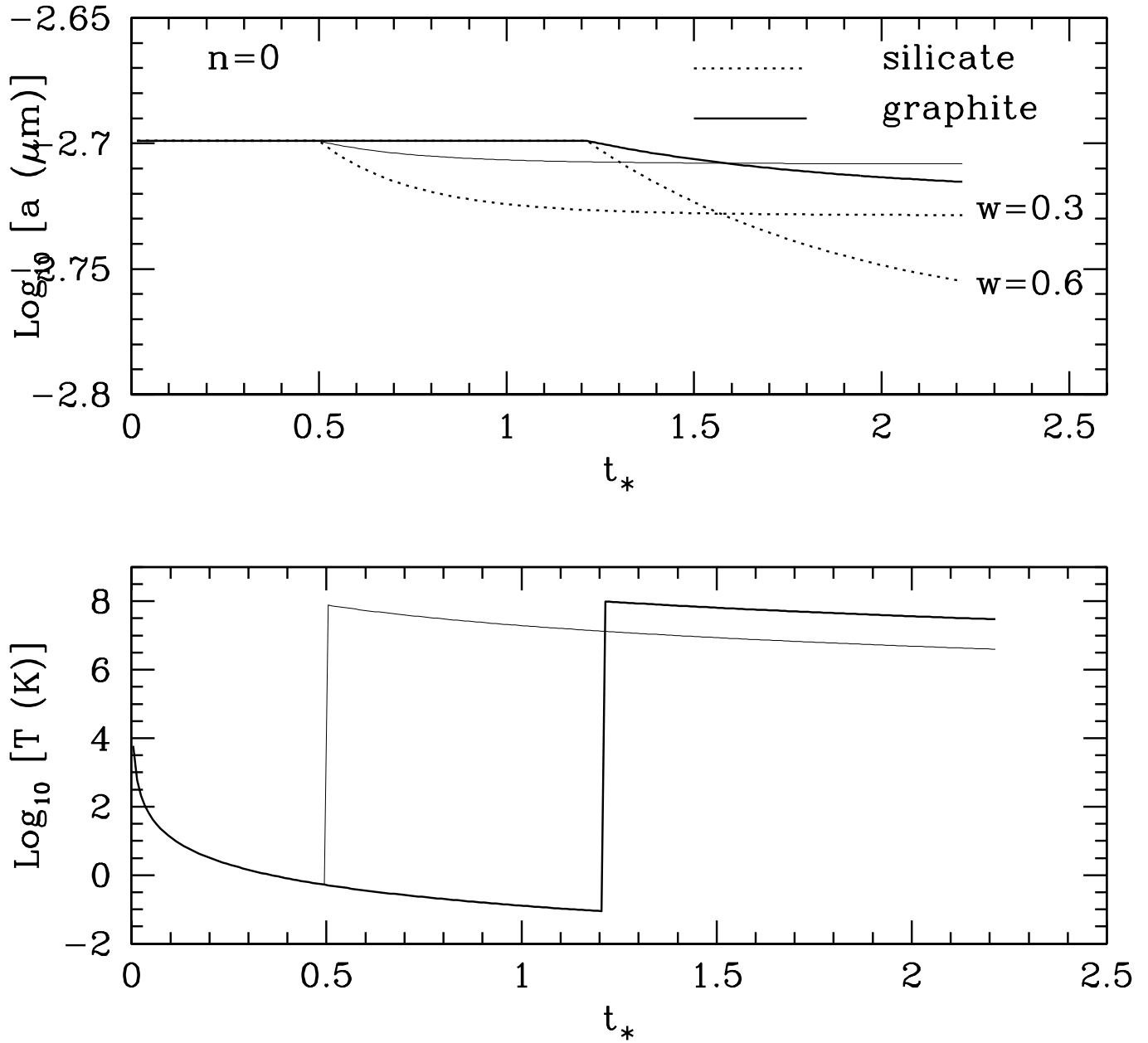


FIG. 1.— The dust grain size as a function of time (where $t_* = t/t_{ch}$) is plotted for $n = 0$, $E = 10^{51}$ erg, $M_{ej} = 10^{34}$ g in the upper panel, for two shells, with $w = 0.6$ and $w = 0.3$. The shell $w = 0.3$ is inside of $w = 0.6$ shell, and is hit by the reverse shock at a later time. The initial grain size (solid line for graphites, and dotted, for silicates) is $1.3 \times 10^{-3} \mu\text{m}$. The bottom panel plots gas temperature as a function of t_* showing the rise at the instant of the reverse shock meeting the two particular shells. ($t_{ch} \sim 1.7 \times 10^3 n_0^{-1/3}$ yr.)

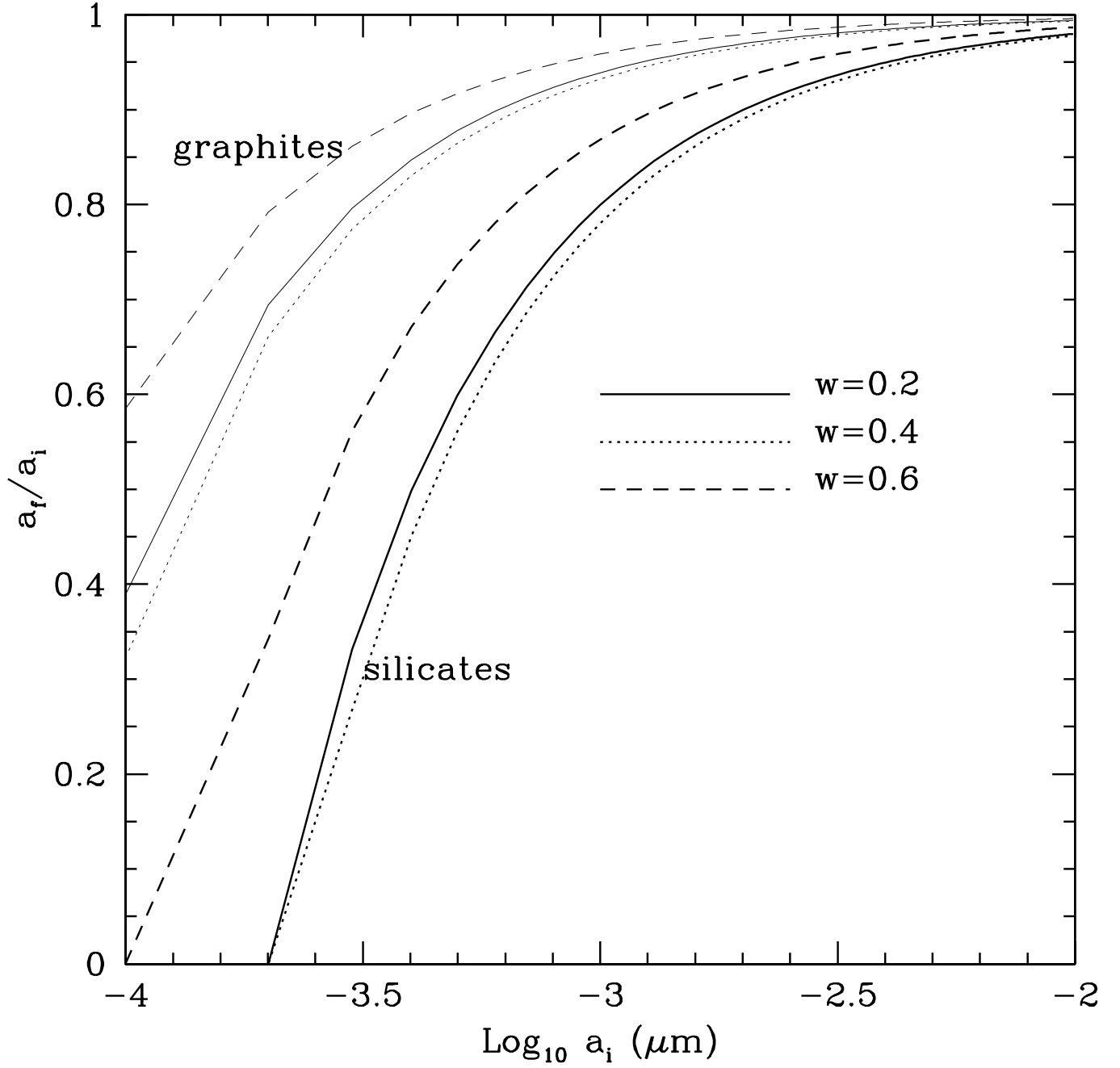


FIG. 2.— Ratio of final to initial grain radius is plotted against initial grain radius (in μm) for silicates (thick lines) and graphites (thin lines), for grains in shells $w = 0.2$ (solid), $w = 0.4$ (dotted), $w = 0.6$ (dashed) for the case of $n = 0$.

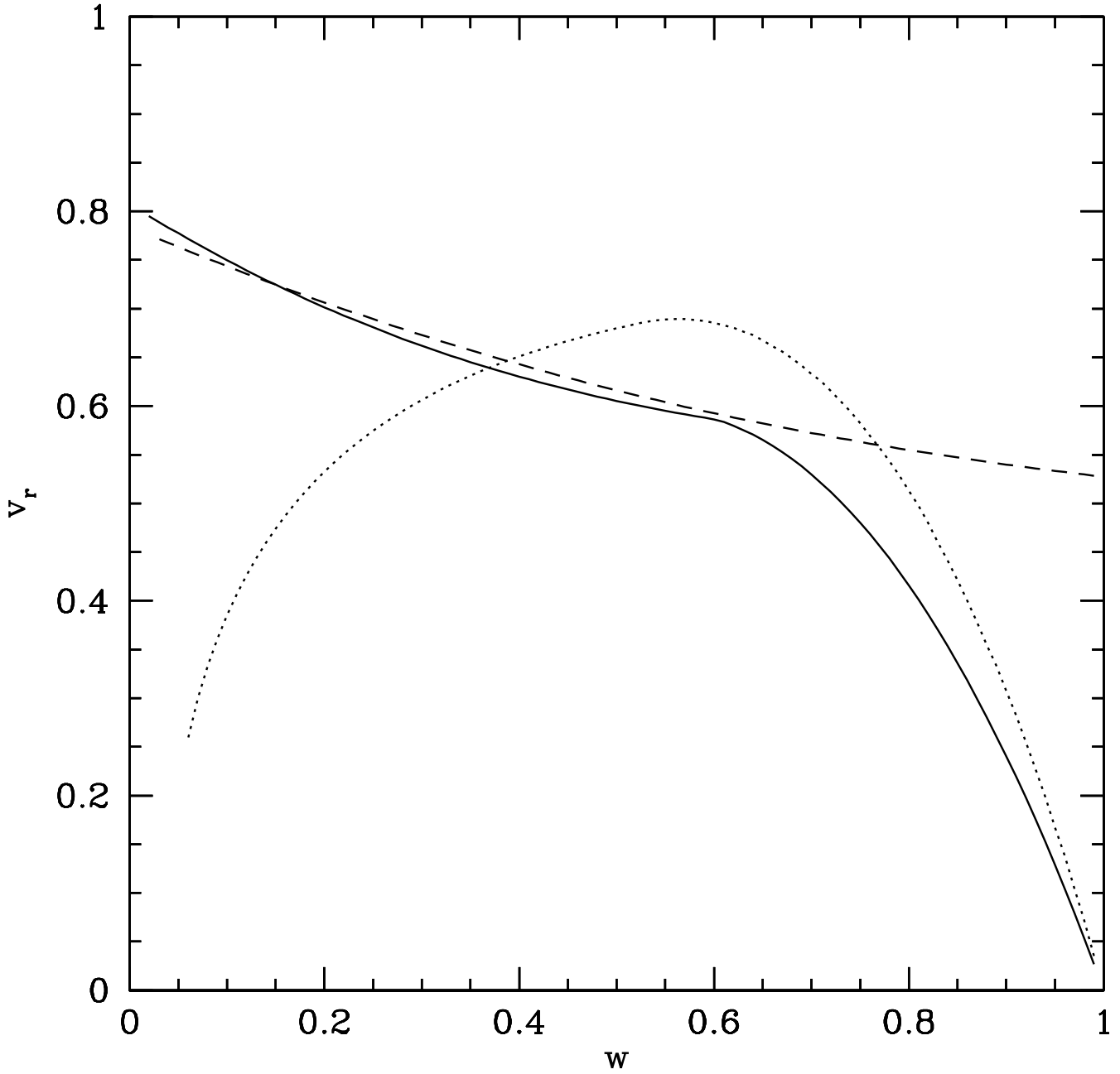


FIG. 3.— The dimensionless velocity of reverse shock in the frame of unshocked ejecta, \bar{v}_r^* (in the units of the characteristic velocity v_{ch}) is plotted against w for $n = 0, 2, 6$ (solid, dotted, dashed lines). For reference, the value of $v_{ch} \sim 3162 \text{ km s}^{-1}$, for $E = 10^{51} \text{ erg}$ and $M_{ej} = 10^{34} \text{ g}$.

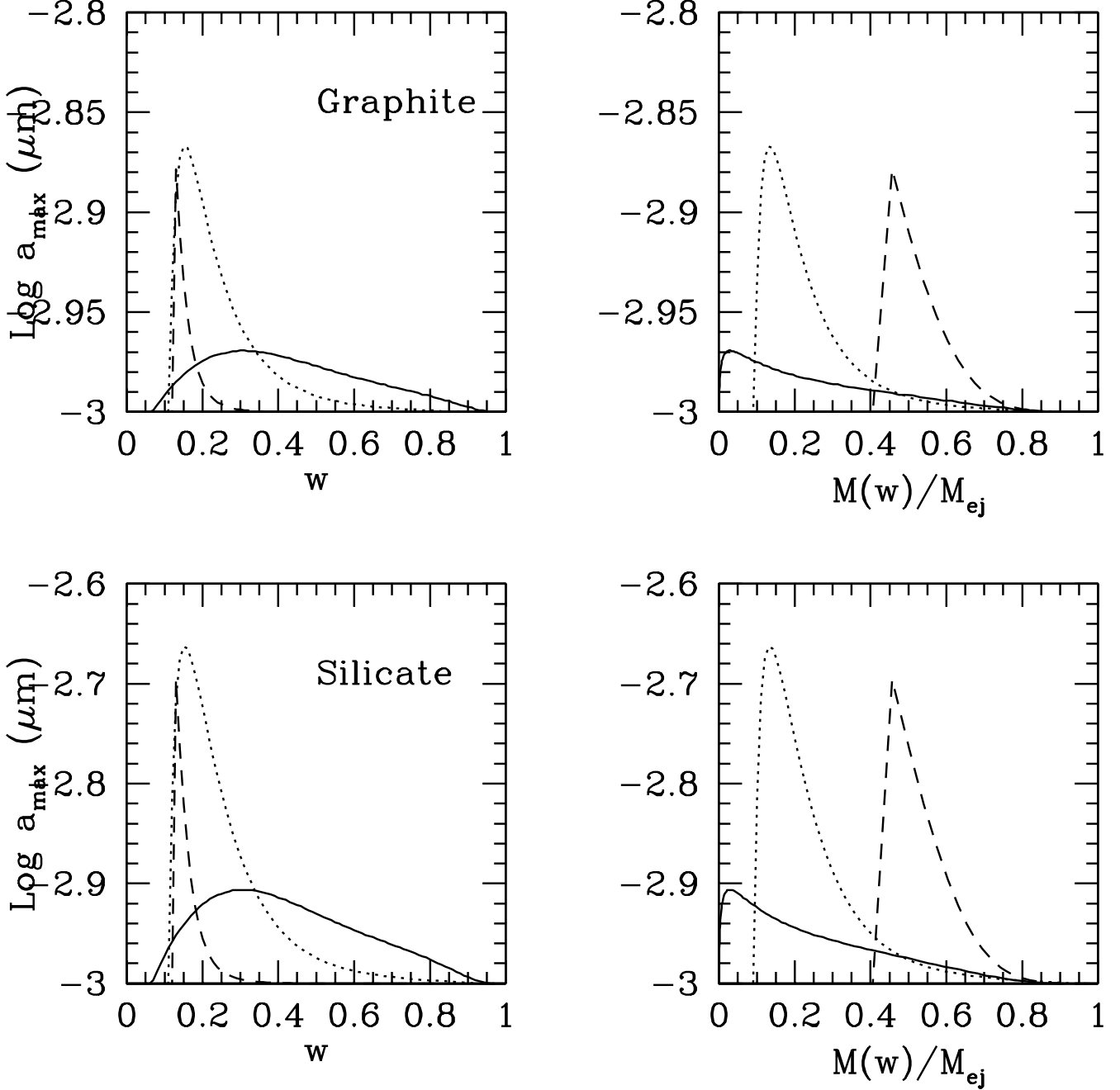


FIG. 4.— The values of maximum size, $\log a_{\text{max}}$ (in μm), below which grains are sputtered below 10^{-7} cm are shown against the parameter w in the left panels, and against the fraction of ejecta mass inside the corresponding shell, $M(< w)/M_{\text{ej}}$, in the right panels. ($w = R(t)/(v_{\text{ej}}t)$, or equivalently, it is the ratio of the velocity of the ejecta in the shell to the maximum ejecta velocity.) The case of graphites are shown in upper panels and the case of silicates, in the lower panels. Dust is introduced at 10 yr, where the tracks begin. Solid, dotted, and dashed lines refer to the cases $n = 0, 2, 4$ respectively. The energy of explosion is assumed to be $E_{\text{ej}} = 10^{51}$ erg and ejecta mass is assumed to be 10^{34} g.

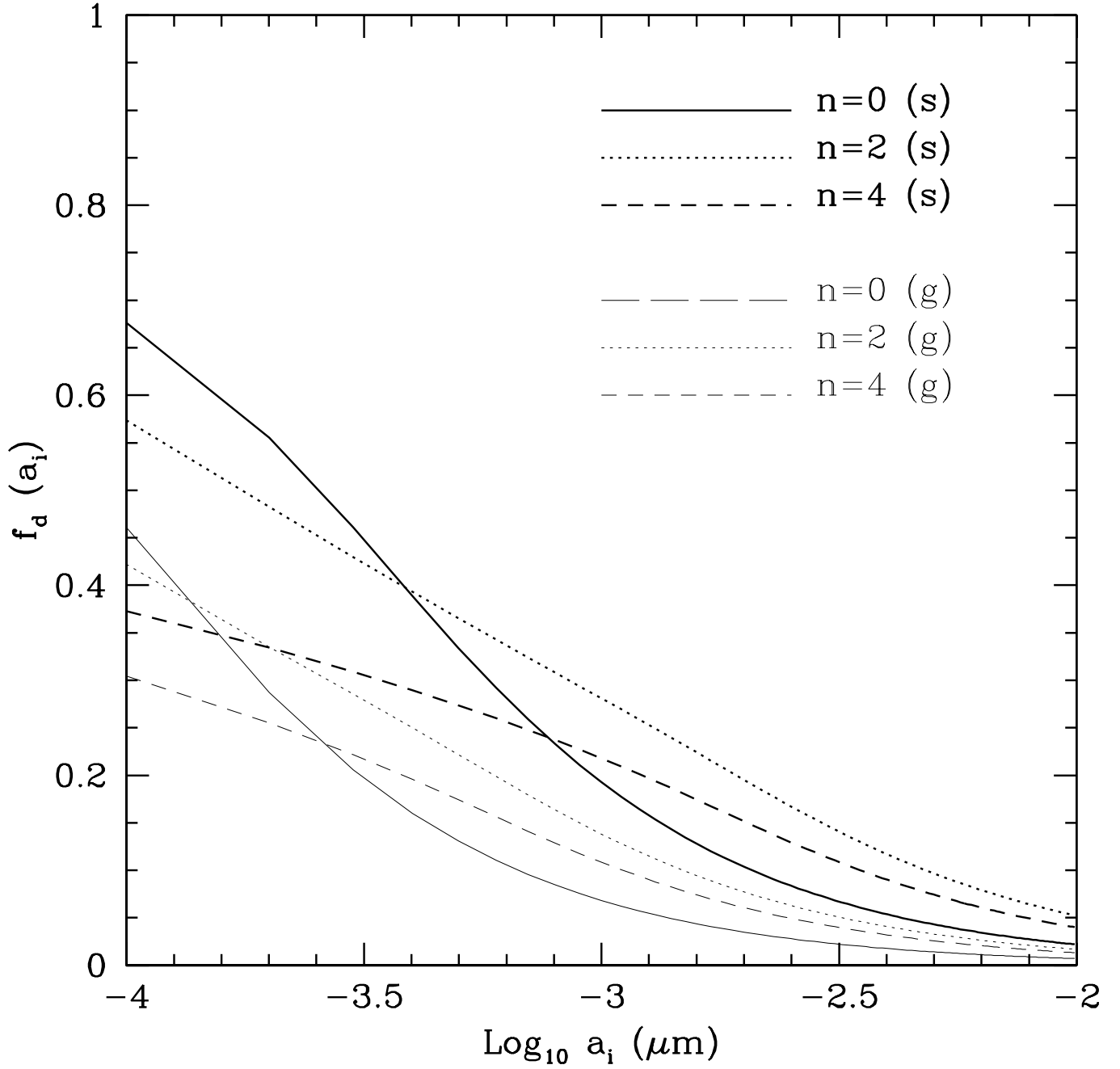


FIG. 5.— Fraction of dust mass sputtered as a function of initial grain size, weighted by the mass of the shell in which they are formed, for $n = 0$ (solid), 2 (dotted) and 4 (dashed), for silicates (thick curves) and graphites (thin curves).

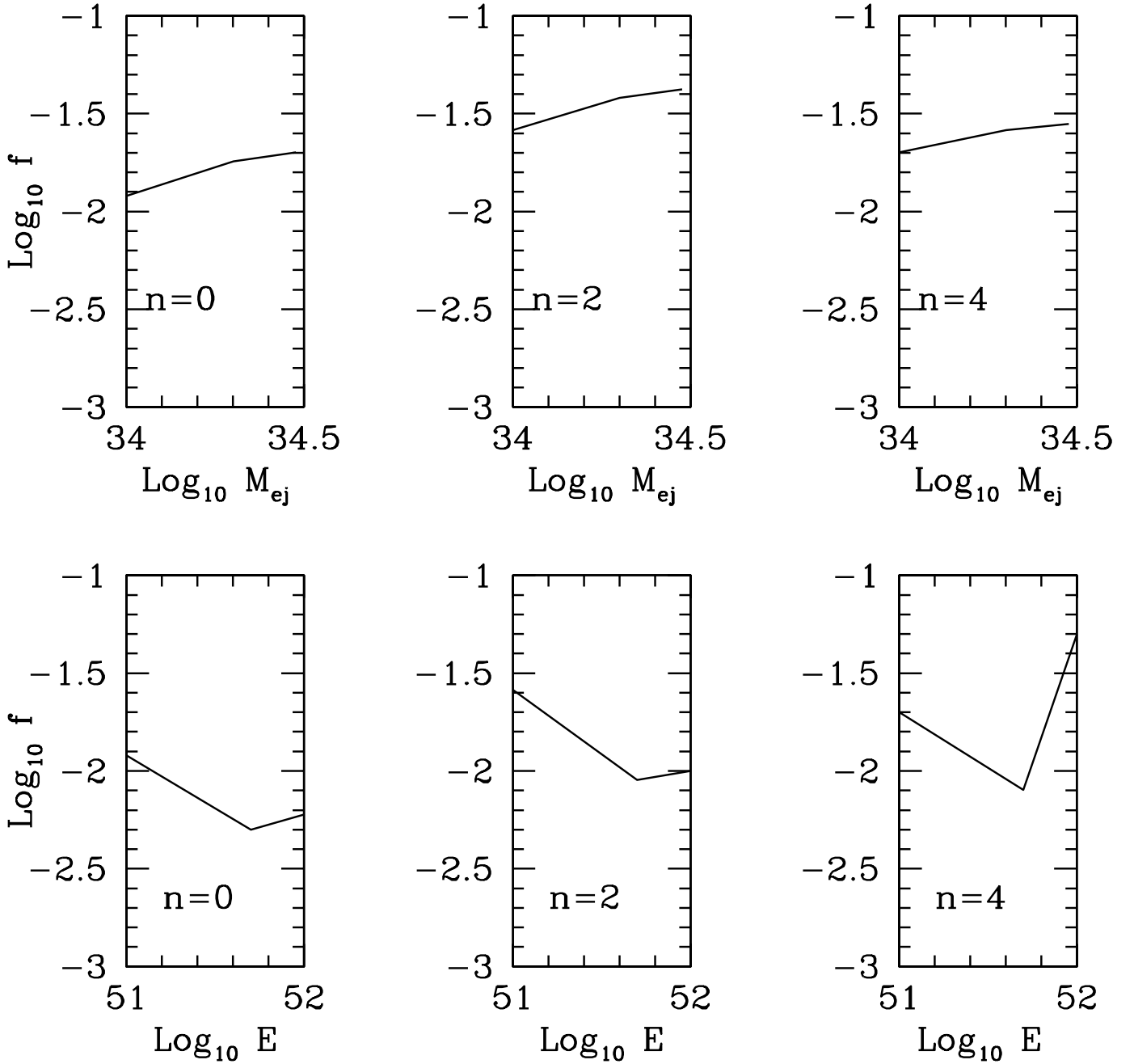


FIG. 6.— Fraction of dust mass sputtered is plotted in the upper panel as a function of mass of ejecta, keeping the explosion energy constant at 10^{51} erg, for different values of n . In the lower panel, the fraction of destroyed dust mass is plotted (for different n) as a function of explosion energy E , keeping the ejecta mass constant at 10^{34} g.